Load-following, co-generation, and sensor placement strategy for small modular reactors

UPADHYAYA Belle R.[1], LI Fan[2], PERILLO Sergio R.P.[3], and HINES J. Wesley[1]

1. Nuclear Engineering Department, University of Tennessee, Knoxville, TN, 37996-2300 USA (bupadhya@utk.edu)
2. Altran Solutions, Norcross, GA 30092 USA
3. IPEN, 05508-900 São Paulo, BRAZIL

Abstract: The deployment of next generation nuclear power plants will include small modular reactors (SMR) that range in electricity production from 50 MWe to 200 MWe. A key to economic and sustained operation of these systems would be the ability to monitor components and devices on-line, and to incorporate autonomous control of these systems. The development of control strategies for multiple-module systems and the allocation of sensors to optimize fault detection and diagnosis are presented with application to a nuclear desalination system using integral SMRs as the heat source. The design performance is evaluated using MATLAB-SIMULINK based reactor dynamic models.
Keyword: small modular reactors; steam mixing; fault diagnosis; nuclear desalination; sensor placement

1 Introduction

The nuclear power industry is undergoing a rapid growth in the deployment of light water reactors and gas-cooled reactors, ranging in electricity production from 50 MWe to 1500 MWe. The research, development, and demonstration work presented in this paper is focused on small modular reactors (SMR) [1]. These range in power output from 50 MWe to 200 MWe. The reactor design of interest is the integral pressurized water reactor, with possibly multiple modules that operate in parallel and feed steam to a single turbine. Such a configuration requires mixing steam from two or more modules in a steam header, with steam from all the units maintained at the same conditions. The efficient operation of this configuration requires advanced control strategy and sensor allocation for optimal anomaly tracking and fault isolation. The thermal output is also partitioned to provide process heat to systems such as desalination plants and district heating.

The research work at the University of Tennessee is to develop control strategies for reactor operation at different power levels, load following capability for the partitioning of process heat, and the design of sensor placement for effective fault monitoring and diagnosis. Both classical control methods and model-predictive controllers were developed for single unit operation. The optimal sensor placement approach uses the criterion for fault detectability and fault isolation, with a constraint on the total resources available. A digraph-based approach for relating the measurements, using a physical model of the sub-system under consideration, is used for developing a criterion function.

These control and sensor optimization methods are applied to a 350 MWe integral pressurized water reactor, the International Reactor Innovative and Secure (IRIS), developed by Westinghouse Technology Center [2]. The results demonstrate the automated design features of control and instrumentation strategies, which can also be implemented for other SMRs.

The control strategy for steam mixing and load following operation with a dual-module reactor plant are described in section 2. The theory and algorithms for optimal sensor allocation and fault diagnosis are outlined in section 3. Concluding remarks are presented in section 4.

2 Multi-modular reactor concept and control strategy

2.1 General concept of a multi-modular plant

A multi-modular reactor system consists of two or more nuclear power units that operate in parallel, with the steam from different units flowing into a

Received date: November 6, 2011
(Revised date: November 12, 2011)

common header. Such power generating stations have the advantages of providing continuous power supply even when one of the units is down for maintenance, and load following features with the modules operating at different power levels. In this study a 1000-MWth Pressurized Water Reactor (PWR) is considered. This Westinghouse PWR is referred to as the IRIS and supplies about 350 MWe power.

The primary and secondary (steam) loops in the IRIS system are incorporated in a large reactor vessel, with the upper head acting as the pressurizer to maintain constant primary pressure. There are eight helical coil steam generators (HCSG) surrounding the reactor core and the riser. The feedwater flow to a pair of HCSGs has a common feed line. The primary water is pumped in a downward direction surrounding the helical tubes. The HCSG is a once-through steam generator producing superheated steam. The reactor control requirements specify constant average coolant temperature across the core and a constant steam pressure. In this work these two control actions are included, thus requiring a multivariate control approach.

The study by Kim and Bernard [3] in the early 1990s focused on the simulation of a U-tube steam generator type multi-modular saturated steam PWR reactor plant capable of operating under normal operational transients with unbalanced loads, and proposed and evaluated a robust, digital closed-loop steam generator level controller for both existing and multi-modular power plants. In Fig. 1, such a proposed twin-module IRIS plant is shown, with the water exiting the reactor core and flowing down through the shell-side of the respective steam generator, and the super heated steam in the tubing flowing to a common steam header and to the steam turbine.

In a U-tube steam generator system, the saturated steam PWR is operated as a constant pressure-constant flow device with programmed core coolant average temperature that increases with increasing load, with reactor control being maintained by a combination of mechanical control rods responding automatically to load changes, and the soluble neutron poison, boric acid (H_3BO_3), responding to fuel burn-up changes [4].

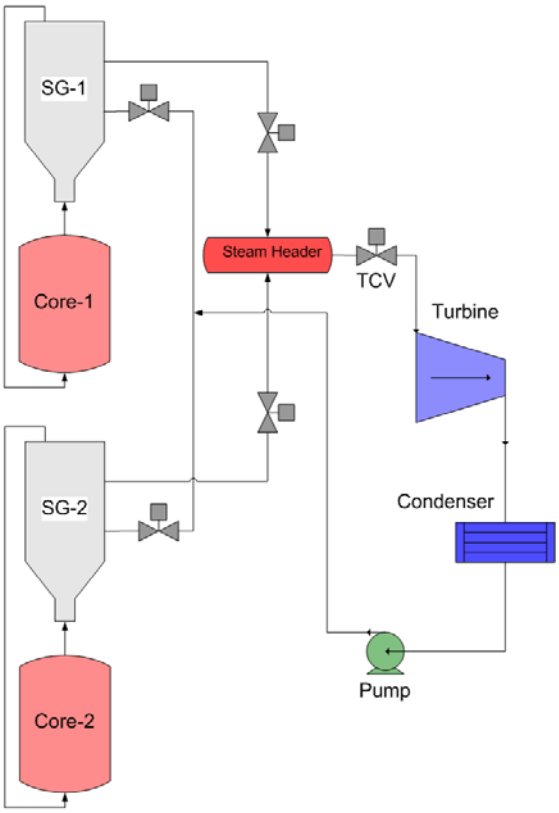

Fig. 1 Configuration of a dual-module nuclear power system with a common steam header.

2.2 IRIS multi-modular control strategy

The multi-modular reactor systems have the advantages of providing continuous power supply even when one of the units is down for maintenance, and load following features with the modules operating at different power levels. This two-unit model is based on the single model and has the same constants, initial conditions, etc, but there are a few differences between the two versions, most notably a second T_{ave} controller and a steam pressure controller. Steam from both the units is superheated and any pressure loss between the steam generator exit and the pressure header is neglected. Also, an additional demand input was added to the model to independently set the power in the second unit. But the most important changes are in some of the assumptions, specifically concerning the calculation of the temperature of the mixed steam. The assumptions are listed below for completeness:

- Unlike in PWRs with recirculation-type steam generators, where there is a sliding T_{ave} controller,

the average of core inlet and outlet temperatures in IRIS remains constant, with a set point value of 310°C (590°F) over the entire simulation.

- The pressure of the steam from the helical coil steam generators (HCSG) remains constant at 5.8 MPa (~841 psi) for the entire range of reactor operation.
- Feed water temperature is fixed at 223.9°C (435°F), corresponding to 100% power for entire simulations.
- There is no feed-forward controller to quickly move control rods based on changes in power load demands.
- Pressurizer and balance-of-plant models are not included in the simulation. These parameters are assumed to be at fixed values.
- Steam generator feed water flow rate is set by a power demand – feed flow program based on a FORTRAN code developed by North Carolina State University (NCSU) [11].
- Steam mixture temperature at the steam header is calculated assuming constant pressure (see bullet above), balance of mass and steam properties, and is calculated as:

$$h_T(t) = \frac{h_1(t)\dot{m}_1 + h_2(t)\dot{m}_2}{\dot{m}_T} \quad (1)$$

$$\dot{m}_T = \dot{m}_1 + \dot{m}_2 \quad (2)$$

Where:

$h_T(t)$ is the temperature-dependent total enthalpy.

$h_1(t)$ and $h_2(t)$ are unit #1 and unit #2 temperature-dependent enthalpies, respectively.

$\dot{m}_T$, $\dot{m}_1$, $\dot{m}_2$ are total, unit #1 and unit #2 mass flow rates, respectively. More details are given in Ref [11].

The values of $h_T(t)$ obtained from the combined steam temperatures are then used to determine the temperature of the mixed steam at the corresponding superheated steam pressure of 5.8 MPa (841 PSI) using a look-up table embedded in the Simulink model, assuming steam outlet pressure deviations can be neglected.

2.3 Multi-modular IRIS plant used in load following maneuvers

As stated earlier, load following is the capability of a reactor to follow changes in the grid demand; for example, reduced consumption over the weekend or load changes during the day. Hence, it is desirable from an economical point of view that a multi-modular reactor plant also be able to do just that, although there are currently no regulations in this regard. For this purpose, the two-unit model with steam mixing is subjected to transients similar to the power demand profile, shown in Fig. 2. However, only the first 30 out of the 60 hours of such profile were simulated for three main reasons: running the whole profile is not necessary (thus avoiding repetition), it is time consuming and possible numerical stability issues.

The results shown are for the two-unit model using profile 1 (Fig. 2) load demand for module #1 and profile 2 (Fig. 3) load demand for module #2. The programmed feed water flow rate to module #2 is shown in Fig. 4. Note that the feed flow rate to module #1 is constant. The steam flow rate follows the feed water flow rate profile. The feed water flow rates in the two modules follow the power demand and eventually match the steam flow rate in the two modules. Figures 5 and 6 show the changes in the average primary coolant temperature (T_{ave}) in modules #1 and #2 around their respective set points. In Figs. 5 and 6 T_{ave} varies by about 2°C and follows the load demand as the controller changes the external reactivity. Hence, the core inlet and outlet temperatures adjust to maintain a constant average coolant temperature around the set point. The changes in the steam temperature at each of the reactor modules and the temperature of the mixed steam in the common header are shown in Fig. 7. The two power levels have different steady state profiles and the steam temperature does not match during these transients. The figure shows the temperature of the steam in the steam header where the two streams mix and supply the steam to the turbine. As the power in either of the modules decreases, the area available for heat transfer in the steam generator increases, therefore increasing steam temperature; conversely, the steam temperature decreases following a power increase. The control strategy of regulating the average reactor temperature and the steam pressure is robust for this load following operation. The controllers are capable of maintaining both average moderator temperature and steam outlet pressure around their set points in both the modules.

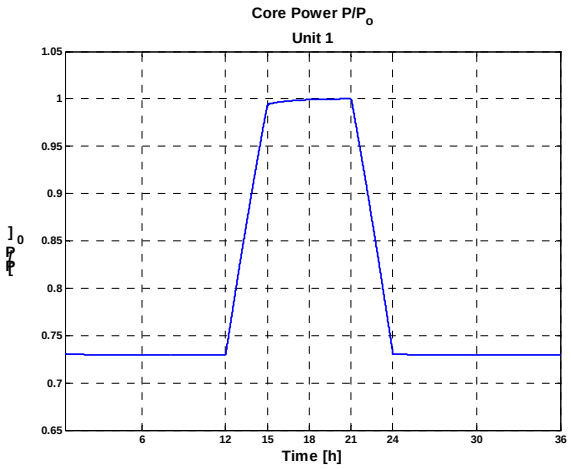

Fig. 2 Reactor module #1 power profile in percent full power.

Fig. 3 Reactor module #2 power profile in percent full power.

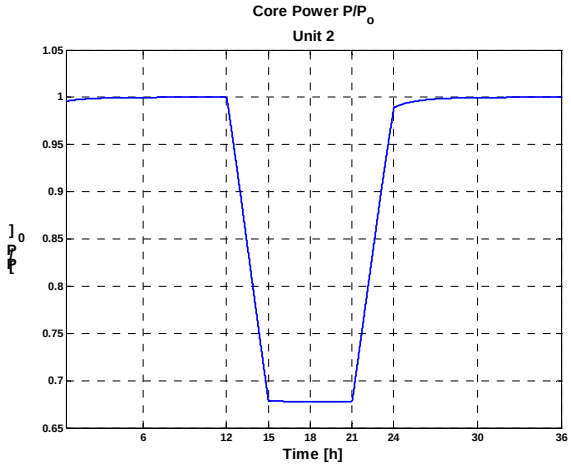

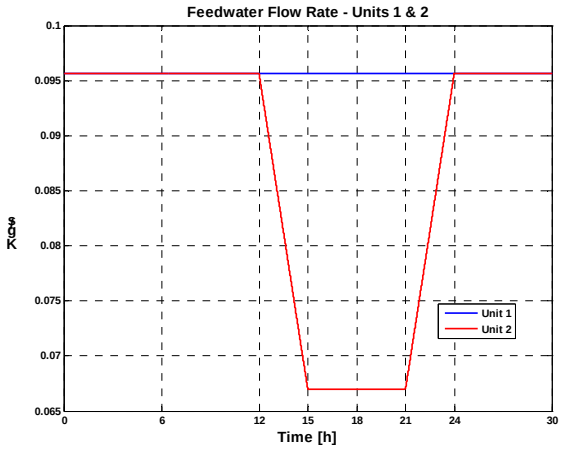

Fig. 4 Feed water flow rates to modules #1 and #2.

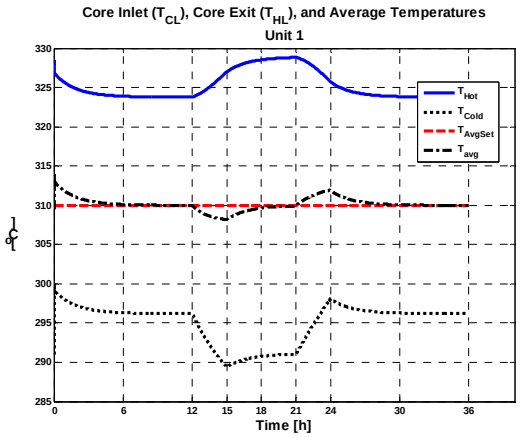

Fig. 5 Reactor module #1 average moderator temperature.

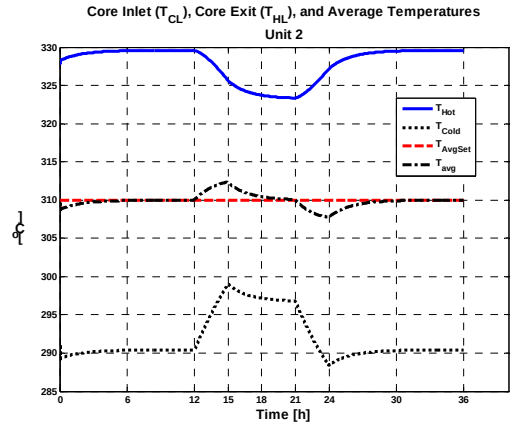

Fig. 6 Reactor module #2 average moderator temperature.

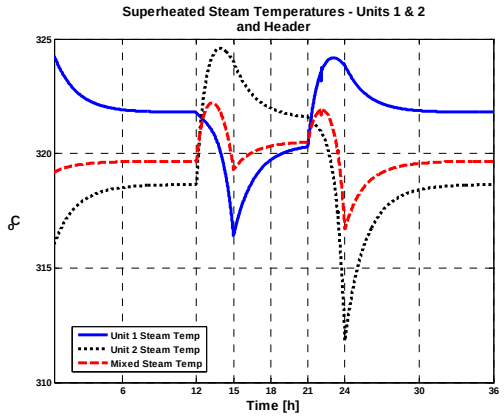

Fig. 7 Units #1, #2, and mixed steam header temperatures.

Ref [11] provides further details of this analysis.

2.4 Model robustness

Four different perturbation cases were investigated to analyze the model's capability of detecting small perturbations, thus testing its robustness and sensitivity [11].

Case 1:

- 2.8°C (5°F) step perturbation in T_{cold} temperature measurements in module #1 at t=6h, with both modules operating in steady state at 100% power.

Case 2:

- 1.7°C (3°F) step perturbation in T_{cold} temperature measurements in module #1 at t=6h, with both modules operating in steady state at 100% power.

Case 3:

- 1% Full Scale (FS) random perturbation in feed water flow rate at t=6h for 5 minutes in both modules. Module #1 operating at 90% and module #2 at 95%.

Case 4:

- 1% FS perturbation in feed water flow rate in module #1 at t=6h. Module #1 operating at 95% and Module #2 at 100%.

Cases 1 and 2 involve sensor perturbations, in which the source of perturbation is not in the process itself but in the sensor measurements, but is propagated throughout the system. On the other hand, cases 3 and 4 involve process perturbations due to hypothetical equipment malfunctions, and such perturbations do propagate throughout the process. Figure 8 shows the variations in the steam temperatures for the case of a 1% FS perturbation of feed water flow in module #1. The response of the steam generator dynamics indicates a robust behavior of module #1 steam temperature and the steam header temperature. The bias created in the steam header temperature is less than 0.3°C.

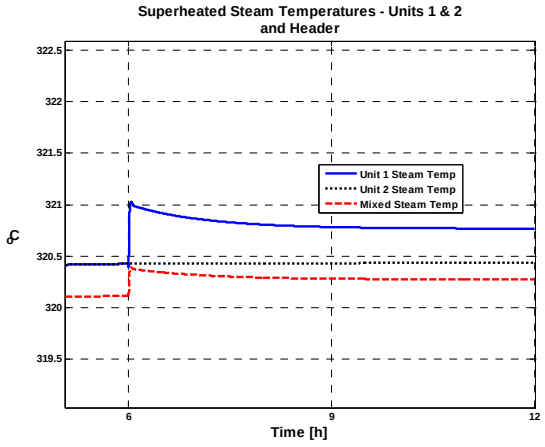

Fig. 8 Steam header temperature variation for a negative 1% feed water flow rate in module #1

3 Optimum sensor placement algorithms and applications

3.1 Introduction

Sensor placement design is a critical component of a fault diagnostic system. Whenever a process encounters a fault, the effect of the fault is propagated to some or all of the process variables. The main objective of the fault diagnosis is to observe these fault symptoms and determine the root cause of the observed behavior. The ability of the sensor network to detect and discriminate failure modes and anomalous conditions is crucial for the efficiency of the fault diagnostic system. With hundreds of process variables available for measurement in a nuclear power system, the selection of optimum sensor locations poses a unique problem.

The objective of this research is to design an efficient sensor placement strategy that will help in the quick and accurate identification of faults. The solution to the problem of sensor placement may be broadly divided into two tasks: (1) fault modeling or prediction of cause-effect behavior of the system, generating a set of variables that are affected whenever a fault occurs, and (2) use of the generated sets to identify sensor locations based on various design criteria. In general, given a process with its faults and measurable variables (where sensors may be placed), the cause-effect information is represented in a fault-sensor maximum connectivity matrix. This bipartite matrix serves as the basis for the generation of the fault sets.

The fault propagation or cause-effect behavior can be derived on the basis of the qualitative model that is used to represent the process. The directed graph (DG) is such a qualitative model that can be used to infer the cause-effect behavior in a system. It normally consists of a set of nodes and directed branches. The nodes represent process variables and the branches represent the causal influences between the nodes. Analysis of cause-effect behavior is straightforward in a DG representation as the occurrence of a fault in a DG causes the variables associated with that fault to acquire abnormal states.

3.2 Fault observability and resolution criteria

Fault observability refers to the condition that every fault defined for the process has to be observed by at least one sensor. Given a process DG, the observability problem becomes one of finding the minimum number of sensors that would cover all the faults (root nodes). This is commonly known as "minimum set covering problem" [5], where the sets to be covered are the sets of sensors affected by each fault. Resolution refers to the ability to identify the exact fault that has occurred. The maximum resolution that can be attained is restricted by the topology of the DG and the position of the fault or root nodes in the DG. Hence, given the constraints on measurement points, the problem of resolution is that of generating sensor locations so that every fault is resolved to the maximum extent possible. This condition is referred to as the "highest fault resolution". Also, the assumption of single-fault or multiple-fault would lead to different resolutions. For multiple-fault resolution, new "virtual fault" sets which are used to distinguish among faults are formed, in addition to the original sets of nodes affected by each fault. Thus, the resolution problem reduces to finding a cover for these new sets, as well as the original sets. For instance, let A_i denote the set of nodes connected to the i_{th} fault among a set of fault nodes. The causal set should also include a set of virtual faults $B_{ij} = A_i \cup A_j - A_i \cap A_j$ for all i and j, each of which denotes a pair of fault nodes i and j to be distinguished.

The fault observability and resolution problems could be solved exactly by enumeration, but with an increasing number of root nodes and sensor locations, it may not be computationally feasible to solve the problem in that fashion. In many instances, one may only be interested in a "good enough" solution rather than an exact solution. In these cases, heuristics often give a quick and reasonably accurate solution. A *greedy* search heuristic has been developed for solving the single and multiple fault observability and resolution problem. More details concerning *greedy* search heuristics may be found in references [6] [7].

In many cases, it is found that some faults are still indistinguishable using the sensor set obtained from the above sensor placement scheme. Nonetheless, optimal sensor placement design from a fault diagnosis perspective will provide valuable information to the principal component analysis (PCA)-based fault detection and isolation (FDI) system, as later revealed in the case studies. The overall method as described in the preceding sections thus consists of the following steps:

(a) Define all the faults of interest in the process (including process fault and sensor fault) based on the operation history records and available process knowledge; then build DG models of the monitored process, which can be implemented by using empirical relationships or fundamental mathematical model of the process.

(b) Solve the fault observability and resolution problems to decide the allocation of sensors. The obtained sensor set would partially guarantee the detection and isolation of all the faults defined in the first step.

(c) Highlight the faults that cannot be isolated by the information provided by the DG model and the sensor network obtained in steps (a) and (b). These faults will be left to the PCA fault diagnostic system for further detection and isolation.

3.3 Principal component analysis (PCA)

PCA is a statistical algorithm of dimension reduction by projecting data on to a lower dimensional space such that the major variation of the original data can be preserved. Given a normalized process data matrix X ($m \times n$) composed of m observations with n measured variables. PCA decomposes X into two components, a predicted value $\hat{X}$ and an error value E, which determine two orthogonal subspaces, i.e., the principal component (PC) subspace and the residual component (RC) subspace, respectively.

$$\begin{aligned} X &= \hat{X} + E \\ \hat{X} &= TP^T \\ E &= T_E P_E^T \end{aligned} \tag{3}$$

where P is the orthogonal loading matrix and T is the score matrix. The scores T in the PC subspace explain the dominant variation of the measured variables, and the scores T_E in the RC subspace represents the insignificant variation due to model reduction error. The column vectors of principal component loadings P ($n \times l$) are the eigenvectors

corresponding to the l largest eigenvalues of the correlation matrix of the data matrix X and the columns of P_E are the eigenvectors corresponding to the smallest $n-l$ eigenvalues.

Building a model to characterize the relationships among the various measurements is an essential part of the FDI methodology. Patterns of the residuals that signify the mismatch between the model and the actual data most likely correspond to faults of a particular type. Specifically, different faults would cause the corresponding residuals to orient toward different directions. These various prediction error directions are referred to as the fault directions, and the particular fault may be isolated as the one with maximum projection on the enumerated set of fault directions. The proposed fault isolation scheme is described as follows [8].

Let $F = [f_1\ f_2\ f_3 \ldots f_R]$, where $f_1\ f_2\ f_3 \ldots f_R$ are column vectors and denote the fault directions for the various fault scenarios that are observed in an existing database. These fault directions can be extracted from the historical data using clustering techniques. The fault direction f_i in the fault matrix F represents the direction in the residual space for the i_{th} fault such that the samples corresponding to the fault have the maximum projection on f_i. In other words, if E_i denotes the residuals for samples corresponding to the i_{th} fault, the optimization problem is defined as

$$J = \max_{f_i} f_i^T E_i^T E_i f_i \tag{4}$$

subject to the constraint

$$f_i^T f_i = 1 \tag{5}$$

Using the Lagranian multiplier and differentiating J with respect to f_i and setting the derivative to zero for maximization, we get

$$E_i^T E_i f_i = \sigma f_i \tag{6}$$

The fault direction f_i is thus obtained as the first eigenvector of $E_i^T E_i$. The singular value decomposition (SVD) may be used to obtain the eigenvector.

Once the fault matrix F is properly defined, fault isolation is accomplished by calculating the projections onto F and classifying the fault as the one with the maximum projection norm. A fault isolation index for the i_{th} fault is defined as

$$FI_i = 1 - Q_i / Q \tag{7}$$

where

$$Q_i = e(I - f_i f_i^T)(I - f_i f_i^T)e^T \tag{8}$$

In the above equations, Q_i is the distance of the sample from the origin after subtracting the projection of the residuals on the fault direction f_i. It represents the sum of squares of residuals remaining after removing the contribution from the i_{th} fault direction. The fault isolation index quantifies the fraction of Q that is due to f_i. When the j_{th} fault occurs, the projection of the residuals on f_j would be very high. In other words, FI_i would be the largest and nearly 1 for *i=j*, where *i* varies from 1 to *R*. This results in the isolation of the faults from the various existing scenarios.

3.4 Application to multi-stage flash desalination systems

Among a variety of desalination technologies, multi-stage flash (MSF) contributes substantially to the desalinating capacity in the world. Market share of the MSF processes accounts for 70% of all seawater desalination processes [9]. The MSF process usually includes a number of flashing stages connected to a brine heater. Figure 9 illustrates the flow diagram of a simplified MSF system with two flash stages and a brine heater [10]. Seawater feed passes through tubes in each flashing stage where it is progressively heated. Final seawater heating occurs in the brine heater by the heat source. Subsequently, the heated brine flows through nozzles into the first stage, which is maintained at a pressure slightly lower than the saturation pressure of the incoming water. As a result, a small fraction of the brine flashes, forming pure steam.

The heat needed to flash the vapor comes from cooling of the remaining brine flow, which lowers the brine temperature. Subsequently, the produced vapor passes through a mesh demister in the upper chamber of the

flashing stage where it condenses on the outside of the condensing brine tubes and is collected in a distillate tray. The heat transferred by the condensation warms the incoming seawater feed as it passes through that stage. The remaining brine passes successively through all the stages at progressively lower pressures, where the process is repeated. The hot distillate flows as well from stage to stage and cools itself by flashing a portion into steam which is re-condensed on the outside of the tube bundles.

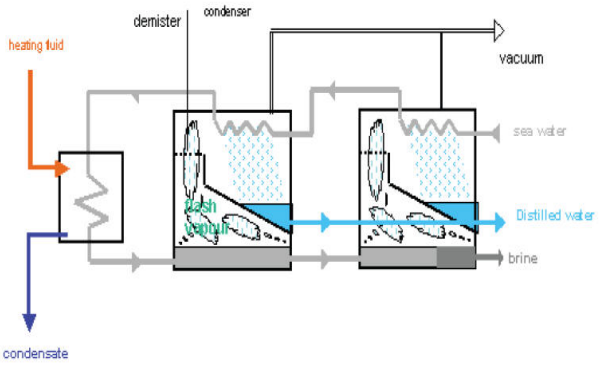

Fig. 9. Schematic diagram of an industrial MSF design [10].

The DG model of the simplified MSF system [12] is shown in Fig. 10. The yellow F nodes represent the root nodes of the system, each of which corresponds to a fault. The 27 measurements that are available are listed in Table 1. Table 2 lists eight fault cases that need to be monitored. The fault diagnosis of the simplified MSF system takes into account the sensor faults, process faults, and controller faults. The four sensor faults are all sensor drifts; the heat transfer degradation faults of flash stages #1 and #2 are considered to be process anomalies in the MSF system. Changes in the set points of the top brine temperature (TBT) controller and the brine level controller of stage #2 are identified as the two controller faults for the desalination process. As can be seen, the digraph has clearly illustrated the cause-effect relationships among the involved variables and the propagation pathways from the fault nodes to other nodes.

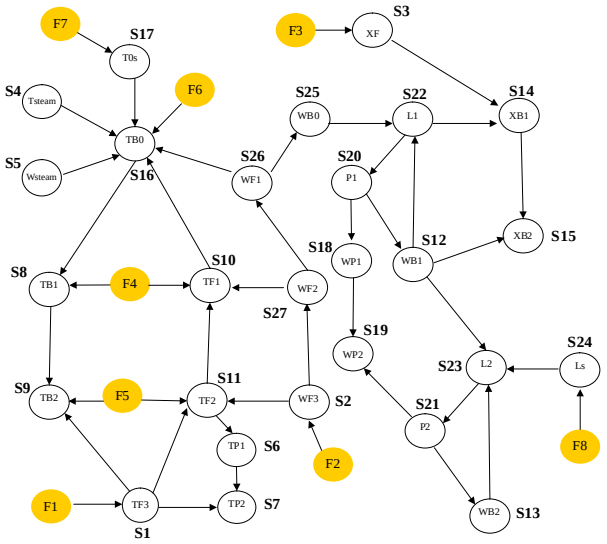

Fig. 10 Directed graph of a two-stage MSF system [12].

Table 1 Two-stage MSF system variables

Index	Description
S1	Inlet cooling brine temperature
S2	Inlet cooling brine flow
S3	Inlet cooling brine salinity
S4	Inlet steam temperature
S5	Inlet steam flow rate
S6	Distillate product temperature exiting stage #1
S7	Distillate product temperature exiting stage #2
S8	Flashing brine temperature exiting stage #1
S9	Flashing brine temperature exiting stage #2
S10	Cooling brine temperature exiting stage #1
S11	Cooling brine temperature exiting stage #2
S12	Flashing brine flow exiting stage #1
S13	Flashing brine flow exiting stage #2
S14	Flashing brine salinity exiting stage #1
S15	Flashing brine salinity exiting stage #2
S16	Top brine temperature
S17	Top brine temperature controller set point
S18	Distillate product flow exiting stage #1
S19	Distillate product flow exiting stage #2
S20	Stage #1 pressure
S21	Stage #2 pressure
S22	Brine level in stage #1
S23	Brine level in stage #2
S24	Stage #2 brine level controller set point
S25	Cooling brine flow exiting the brine heater
S26	Cooling brine flow exiting stage #1
S27	Cooling brine flow exiting stage #2

Table 2 Faults considered for two-stage MSF system

Fault Nodes	System Faults
F1	Inlet cooling brine temperature sensor drift
F2	Inlet cooling brine flow sensor drift
F3	Inlet cooling brine salinity sensor drift
F4	Flashing stage #1 heat transfer degradation
F5	Flashing stage #2 heat transfer degradation
F6	Top brine temperature sensor drift
F7	Top brine temperature controller fault
F8	Stage #2 brine level controller fault

3.5 Results of sensor placement and fault diagnosis

The *greedy* search heuristic is used to find the minimum set of sensors required to observe all the eight faults listed in Table 2 for the two-stage MSF system. It gives nodes $[S_9, S_{15}, S_{16}, S_{23}]$ as the sensor set. Although all the faults can be detected, not every fault can be distinguished from one another.

To obtain the set of sensors that would give maximum resolution under single-fault assumption, additional "virtual faults" have to be created as discussed earlier. Sets A are associated with the original faults. The virtual faults $B_{ij} = A_i \cup A_j - A_i \cap A_j$ are also constructed. This involves generation of $C_8^2 = 28$ virtual faults, so that the system now has 36 faults. Now each B_{ij} is represented as a fault node, and a bipartite graph is constructed between these nodes and the sensor nodes. The *greedy* search based heuristic presented for fault diagnostic observability criterion is applied to the new problem. This gives $[S_1, S_2, S_3, S_8, S_9, S_{10}, S_{11}, S_{12}, S_{15}, S_{16}, S_{17}, S_{23}, S_{24}]$ as the minimum sensor set for complete isolation of the selected faults. The advantage of using this optimized sensor set is that more information about the system is utilized, and some basic properties such as the fault detectability and identifiability are already partially guaranteed before PCA is employed to monitor system behavior.

A normal operation database was generated using a two-stage MSF SIMULINK model. The TBT controller set point and the brine level controller set point in the last flashing stage (Stage #2) were systematically changed one at a time. About 1,728 cases were simulated and the data generated were stored in a database. The list of the measured variables used to develop the PCA model is given in Table 3.

A PCA model is built using the data for the nominal operation case. The nominal operation data matrix is preprocessed by auto-scaling the columns in the data matrix to zero mean and unit variance. This puts all the measurements with their different units on a common unit variance scale. Under normal conditions, small residuals would be generated and limited to a certain range. In the test cases when one or several components in the system are under degradation, the so-called causal relations among these variables will be violated. As a result, the mapping of residuals from residual generators or system models will increase in a specific direction.

Table 3 MSF variables used to develop PCA models

Variable	Description
1	Inlet cooling brine temperature (S1)
2	Inlet cooling brine flow (S2)
3	Inlet cooling brine salinity (S3)
4	Flashing brine temperature exiting stage #1 (S8)
5	Flashing brine temperature exiting stage #2 (S9)
6	Cooling brine temperature exiting stage #1 (S10)
7	Cooling brine temperature exiting stage #2 (S11)
8	Flashing brine flow exiting stage #1 (S12)
9	Flashing brine salinity exiting stage #2 (S15)
10	Top brine temperature (S16)
11	Top brine temperature controller set point (S17)
12	Brine level in the stage #2 (S23)
13	Stage #2 brine level controller set point (S24)

As an example, Fig. 11 shows the residual patterns from the PCA models when there is a drift of 0.2% to 1% nominal value in the inlet cooling brine temperature sensor (Fault 1). The residuals are the differences between the measurement values and their PCA model predictions. Figure 11 also shows a significant increase in the Q statistic of the PCA model exceeding the 95% confidence level. As seen in Fig. 11, the T^2 statistic for the faulty conditions stays within the range. This would be categorized as the fault scenario where the Q statistic is outside the limits and the T^2 statistic is within the limits. These illustrate the capability of data-driven models in detecting system anomalies. It should be kept in mind that both T^2 and Q statistics must be used for fault detection. Either statistic being violated will signify that a fault has happened. Violation of the T^2 statistic represents that the system operates at an abnormal state beyond the model space, while departure of the Q statistic represents that some of the constraint equations defined in the residual space are violated and the system is abnormal.

It is clear that the residuals reflect not only whether there is an abnormal component, but also the severity of the fault, which is important in helping the operator or the automatic controller to select the correct strategy in order to avoid severe negative effect caused by faulty devices. It should be noted that PCA can only deal with steady-state condition or a slow dynamic process. The confidence level will affect the false

alarm. In a real application, the confidence level needs to be adjusted according to the operation requirements.

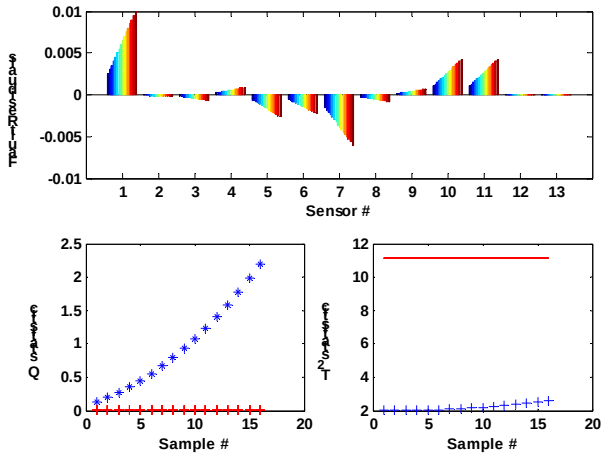

Fig. 11 Residual pattern for inlet cooling brine temperature sensor drift (Fault 1).

The PCA fault direction analysis is performed through processing the fault residuals. The eight fault directions correspond to the eight fault scenarios considered for the MSF system, as listed in Table 2.

Figure 12 shows the fault isolation indices for the case of fault in the inlet cooling brine temperature sensor drift. This is one of the eight fault scenarios in the MSF system. Note that the fault index is close to unity for the particular fault that occurs, and is significantly smaller for the others. Similarly, the other eight fault cases can be diagnosed accurately using this fault isolation approach [12].

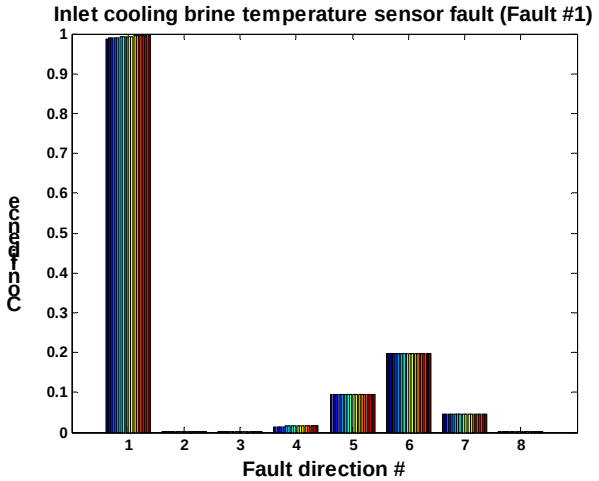

Fig. 12 Fault isolation index for inlet cooling brine temperature sensor drift for a two two-stage MSF.

The PCA directional fault isolation approach can also be extended to simultaneous multiple faults. In this paper, it is assumed that the simultaneous fault occurrence is limited to two at a time for all the eight predetermined faults in the MSF system. The same sensor set is applied to detect and isolate the dual faults. The 8 single-fault directions and the additional 28 dual-fault directions must be used as fault signatures for dual fault isolation. In case of a particular dual-fault, the faulty data are expected to have large projections in the residual space for the two faults involved. As far as the dual-fault direction is concerned, we expect to see the maximum projection of the faulty sample residuals on the corresponding dual-fault direction.

As an example, Fig. 13 illustrates the fault isolation for a particular dual-fault scenario involving Fault #1 and Fault #6. These faults are inlet cooling brine temperature sensor drift and top brine temperature sensor drift. In the top plot, the fault isolation indices for single fault detector are in the range 0.5 – 0.6, with the other fault indices being less than 0.1. Nevertheless, the single-fault directional signatures for the dual-fault are still distinct enough to provide an initial indication of fault isolation. The lower plot in Fig. 13 shows the fault indices for all the 28 dual-fault combinations. Dual fault combination #5 is correctly isolated by the confidence index which is close to unity. Dual fault #5 is the simultaneous occurrence of fault F1 (inlet cooling brine temperature sensor drift) and fault F6 (top brine temperature sensor drift).

In order to apply the PCA fault diagnostic method, it is necessary to pre-define the faults considered for the system of interest. In the event of undefined faults occurring in the system, one may be able to observe the faults using the fault directional approach, but the clear fault isolation may not be achievable with the existing fault directions. These faults, if properly identified later, may be included in the fault set. Thus, when a fault, that is not in the pre-selected set occurs, the confidence indices may have a spread without a clear indication of a specific fault. However, this is still an indication of impending fault, and further analysis is necessary to isolate the fault condition.

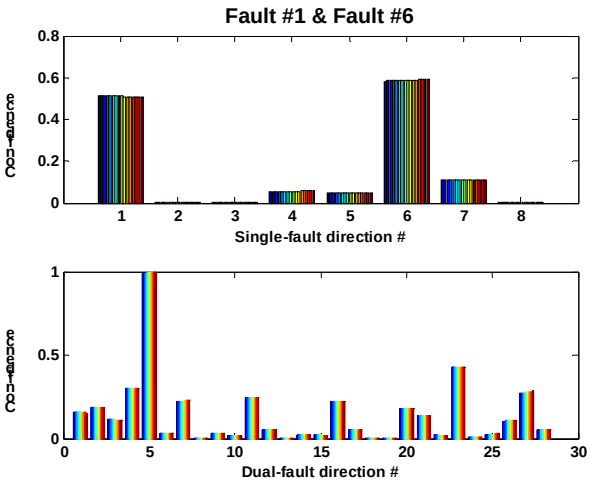

Fig. 13 Fault isolation index for a dual-fault case with simultaneous sensor faults #1 and #6.

4 Concluding remarks

A comprehensive approach for the multivariate control of a dual-module reactor system was presented with application to the IRIS small modular reactor. The results demonstrate the ability of the multi-modular plant to follow load and maintain desired reactor and steam conditions. These results are the first of their kind and are important first steps towards developing small multi-modular reactors of the future.

A general design framework was developed in this work in order to detect and isolate sensor, process, and device anomalies. The optimal sensor selection strategy is also effective in the systematic choice of process measurements for use in fault monitoring and diagnostics algorithms. A PCA method was introduced to generate fault signatures of typical faults defined in a MSF desalination plant. When the optimal sensor sets were used, both sensor faults and process faults were correctly detected and isolated using T^2 and Q statistics, as well as fault isolation index. It was also discovered through the FDI case studies that the PCA fault diagnostic approach could be extended to detect and isolate simultaneous dual-faults using the optimal sensor sets identified for the single-fault cases, in which case both single-fault and dual-fault directions shall be used as fault signatures in order to achieve dual-fault isolation. The fault diagnostic results demonstrated the effectiveness of the developed FDI methods, when used in conjunction with an optimal sensor selection strategy.

Acknowledgments

This research and development was sponsored by a U.S. Department of Energy NERI-C grant with the University of Tennessee, Knoxville.

References

[1] INGERSOLL, D.T.: Deliberately small reactors and the second nuclear era, Progress in nuclear energy, 2009, 51: 589-603.

[2] CARELLI, M.D., CONWAY, L.E., ORIANI, L.: The design and safety features of the iris reactor, Nuclear engineering and design, 2004, 230: 151-167.

[3] KIM, K.K., BERNARD, J.A.: Considerations in the control of PWR-type multimodular reactor plants, IEEE Transactions on nuclear science, 1994, 41: 2686-2697.

[4] LISH, K.C.: Pressurized water reactors, nuclear power plant systems and equipment, ED. Industrial press, 1972: 19-20.

[5] PARKER, R.G., RARDIN, R.L.: Discrete optimization, San Diego: Academic Press, 1998.

[6] RAGHURAJ, R., BHUSHAN, M., RENGASWAMY, R.: Locating sensors in complex chemical plants based on fault diagnostic observability criteria, AICHE journal, 1999, 45: 310-322.

[7] BHUSHAN, M., RENGASWAMY, R.: Design of sensor location based on various fault diagnostic observability and reliability criteria, Computers and chemical engineering, 2000, 24: 735–741.

[8] KAISTHA, N., UPADHYAYA, B.R.: Incipient fault detection and isolation of field devices in nuclear power systems using principal component analysis, Nuclear technology, 2001, 136: 221-230.

[9] EL-DESSOUKY, H.T., ETTOUNEY, H.M., AL-ROUMI, Y.: Multi-stage flash desalination: present and future outlook, Chemical engineering journal, 1999, 73(2): 173-190.

[10] IAEA: Status of nuclear desalination in IAEA member states, TECDOC-1524, International atomic energy agency, Vienna, Austria, 2007.

[11] UPADHYAYA, B.R., PERILLO, S.R.P.: Advanced instrumentation and control methods for small and medium reactors with iris demonstration, vol. 5: Multi-modular integral pressurized water reactor control and operational reconfiguration for a flow control loop. final report prepared for the U.S. department of energy, University of tennessee. Report no. DE-FG07-07ID14895/UTNE/2011-7, MAY 2011.

[12] UPADHYAYA, B.R., LI, F.: Advanced instrumentation and control methods for small and medium reactors with iris demonstration, vol. 4: Dynamic modeling, sensor placement design, and fault diagnosis of nuclear desalination systems. final report prepared for the U.S. department of energy, university of tennessee. Report no. DE-FG07-07ID14895/UTNE/2011-6, MAY 2011.